Inorg. Chem. **2004**, *43*, 2368–2378

Density Functional Investigation of Metal–Metal Interactions in d^4d^4 Face-Shared $[M_2Cl_9]^{3-}$ (M = Mn, Tc, Re) Systems

Germán Cavigliasso[†] and Robert Stranger*[,‡]

Department of Chemistry, Faculty of Science, Australian National University, Canberra ACT 0200, Australia

Received August 12, 2003

The molecular and electronic structures of the d^4d^4 face-shared $[M_2Cl_9]^{3-}$ (M = Mn, Tc, Re) dimers have been calculated by density functional methods in order to investigate metal–metal bonding in this series. The electronic structures of these systems have been analyzed using potential energy curves for the broken-symmetry and other spin states arising from the various d^4d^4 coupling modes, and closed energy cycles have been utilized to identify and quantify the parameters which are most important in determining the preference for electron localization or delocalization and for high-spin or low-spin configurations. In $[Tc_2Cl_9]^{3-}$ and $[Re_2Cl_9]^{3-}$, the global minimum has been found to be a spin-triplet state arising from the coupling of metal centers with low-spin configurations, and characterized by delocalization of the metal-based electrons in a double (σ and δ_π) bond with a metal–metal separation of 2.57 Å. In contrast, high-spin configurations and electron localization are favored in $[Mn_2Cl_9]^{3-}$, the global minimum for this species being the ferromagnetic $S = 4$ state with a rather long metal–metal separation of 3.43 Å. These results are consistent with metal–metal overlap and ligand-field effects prevailing over spin polarization effects in the Tc and Re systems, but with the opposite trend being observed in the Mn complex. The ground states and metal–metal bonding observed for the d^4d^4 systems in this study parallel those previously found for the analogous d^2d^2 complexes of V, Nb, and Ta, and can be rationalized on the basis that the d^4d^4 dimer configuration is the hole equivalent of the d^2d^2 configuration.

1. Introduction

In a series of recent publications[1−7] we have explored metal−metal interactions in a wide variety of face-shared dinuclear metal systems (or $[M_2X_9]^{z-}$ "dimers"), which include 3d, 4d, and 5d transition metals with d^1d^1, d^2d^2, d^3d^3, and d^5d^5 electronic configurations.

These extensive series of $[M_2X_9]^{z-}$ dimers are characterized by a wide range of metal−metal interactions. In species of the second (4d) and third (5d) transition series, the overlap between metal d orbitals is the dominant factor, and these systems typically exhibit strong covalent metal−metal bonds. However, in general, metals of the first (3d) transition series have large spin polarization (exchange) energies, and this has a more significant effect on the electronic structure than orbital overlap between adjacent metal centers, leading to localized electron distributions and weakly coupled metal centers in species such as $[V_2Cl_9]^{3-}$ and $[Cr_2Cl_9]^{3-}$.

In systems with d^1d^1, d^2d^2, and d^3d^3 configurations,[1−5] the electrons involved in metal−metal interactions can be associated with the t_{2g} orbitals of a regular octahedral $[MX_6]^{z-}$ complex. For species involving metals in the Fe, Ru, and Os triad possessing a d^5d^5 configuration,[6,7] the metal−metal interaction also depends on whether a "high-spin" or "low-spin" configuration (associated, respectively, with $[t_{2g}^3e_g^2]$ or $[t_{2g}^5e_g^0]$ configurations in the octahedral monomers) is adopted. The heavier members of this series, $[Ru_2Cl_9]^{3-}$ and $[Os_2Cl_9]^{3-}$, are characterized by low-spin configurations and strong coupling between the metal centers as a result of metal−metal σ bond formation. In contrast, the $[Fe_2Cl_9]^{3-}$ system contains weakly coupled high-spin metal centers with an $S = 5$ ground state corresponding to localization of the metal-based electrons.

The wide range of bonding possibilities makes the theoretical and computational treatment of the electronic structures of $[M_2X_9]^{z-}$ dimers particularly challenging.

* Corresponding author.
[†] E-mail: German.Cavigliasso@anu.edu.au.
[‡] E-mail: Rob.Stranger@anu.edu.au.

(1) Lovell, T.; McGrady, J. E.; Stranger, R.; Macgregor, S. A. *Inorg. Chem.* **1996**, *35*, 3079.
(2) McGrady, J. E.; Stranger, R.; Lovell, T. *J. Phys. Chem. A* **1997**, *101*, 6265.
(3) McGrady, J. E.; Lovell, T.; Stranger, R. *Inorg. Chem.* **1997**, *36*, 3242.
(4) Stranger, R.; Turner, A.; Delfs, C. D. *Inorg. Chem.* **2001**, *40*, 4093.
(5) Stranger, R.; McGrady, J. E.; Lovell, T. *Inorg. Chem.* **1998**, *37*, 6795.
(6) Lovell, T.; Stranger, R.; McGrady, J. E. *Inorg. Chem.* **2001**, *40*, 39.
(7) Stranger, R.; Lovell, T.; McGrady, J. E. *Polyhedron* **2002**, *21*, 1969.

10.1021/ic0349611 CCC: $27.50
Published on Web 03/06/2004

Nevertheless, we have shown in our previous publications[1−7] that density functional theory, in combination with the broken-symmetry approach,[8,9] can accurately describe the entire range of metal−metal interactions, from weak antiferromagnetic coupling through to strong multiply bonded metal centers, as well as encompassing both high-spin and low-spin metal configurations.

The present work extends the computational investigation of face-shared $[M_2X_9]^{z-}$ systems to species possessing a d^4d^4 electronic configuration, namely $[Mn_2Cl_9]^{3-}$, $[Tc_2Cl_9]^{3-}$, and $[Re_2Cl_9]^{3-}$. These dimers are particularly interesting in that they may possess electronic states analogous to those of the $[V_2Cl_9]^{3-}$, $[Nb_2Cl_9]^{3-}$, and $[Ta_2Cl_9]^{3-}$ systems,[5] as the low-spin d^4d^4 configuration can be considered the "hole" equivalent of the d^2d^2 configuration. Furthermore, they may also exhibit similar behavior to the $[Fe_2Cl_9]^{3-}$, $[Ru_2Cl_9]^{3-}$, and $[Os_2Cl_9]^{3-}$ systems,[6,7] as both low-spin and high-spin configurations are possible for the individual metal centers. The investigation of d^4d^4 dimers is also necessary in order to undertake a complete analysis of periodic trends in metal−metal interactions across the entire series of face-shared $[M_2Cl_9]^{3-}$ species, from d^1d^1 through d^5d^5 systems. This is the subject of a separate publication.

In this article, the electronic structures of the $[Mn_2Cl_9]^{3-}$, $[Tc_2Cl_9]^{3-}$, and $[Re_2Cl_9]^{3-}$ systems are analyzed in detail by means of potential energy curves for various broken-symmetry and low-lying spin states arising from the d^4d^4 coupling modes. The relative importance of localized and delocalized electron distributions and of high-spin and low-spin configurations is also explored.

2. Calculation Details

All density-functional calculations reported in this work were carried out with the ADF (2002.01) program.[10−12] Functionals based on the Volko−Wilk−Nusair[13] (VWN) form of the local density approximation[14] (LDA) were utilized, and no gradient corrections or relativistic effects were included, as previous work has shown that these corrections normally result in poorer agreement with the experimental structural data.[2] Basis sets of triple-ζ quality and one polarization function (TZP or type IV), incorporating frozen cores (Mn.2p, Tc.3d, Re.4f, Cl.2p), were employed.[10−12]

Calculations on the $[M_2Cl_9]^{3-}$ systems were carried out using the (full) D_{3h} molecular symmetry, with the exception of the broken-symmetry calculations which employed C_{3v} symmetry and applications of the sum method which required C_{2v} symmetry. For comparison, calculations were also carried out on $[MCl_6]^{3-}$ systems using O_h molecular symmetry.

Calculations were performed on the broken-symmetry and other spin states which were considered to be most relevant to the analysis of the electronic structures of the Mn, Tc, and Re $[M_2Cl_9]^{3-}$ systems.

(8) Noodleman, L.; Norman, J. G. *J. Chem. Phys.* **1979**, *70*, 4903.
(9) Noodleman, L. *J. Chem. Phys.* **1981**, *74*, 5737.
(10) *ADF2002.01*; SCM, Theoretical Chemistry, Vrije Universiteit: Amsterdam, The Netherlands (http://www.scm.com).
(11) Fonseca Guerra, C.; Snijders, J. G.; te Velde, G.; Baerends, E. J. *Theor. Chem. Acc.* **1998**, *99*, 391.
(12) te Velde, G.; Bickelhaupt, F. M.; van Gisbergen, S. J. A.; Fonseca Guerra, C.; Baerends, E. J.; Snijders, J. G.; Ziegler, T. *J. Comput. Chem.* **2001**, *22*, 931.
(13) Vosko, S. H.; Wilk, L.; Nusair, M. *Can. J. Phys.* **1980**, *58*, 1200.
(14) Kohn, W.; Sham, L. J. *Phys. Rev.* **1965**, *140*, A1133.

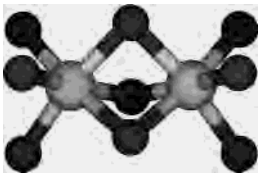

Figure 1. Molecular structure of face-shared $[M_2X_9]^{z-}$ systems.

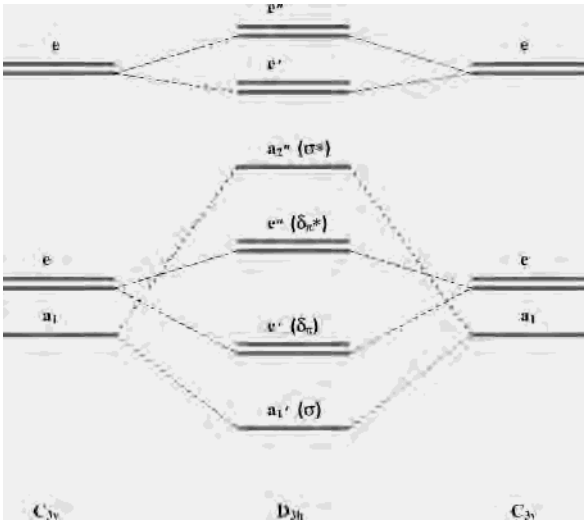

Figure 2. Schematic representation of the correlation between metal-based molecular orbitals in C_{3v} (broken-symmetry) and D_{3h} (full-symmetry) descriptions.

Calculations were not performed on all possible states arising from the various d^4d^4 coupling modes as, in general, many of these states are multideterminantal and thus difficult to describe in terms of density functional theory. In instances where the orbital degeneracy of a particular configuration gives rise to more than one multiplet of the same spin and the sum method could not be applied, calculations were carried out on the "average" of states.

3. Results and Discussion

The theoretical and computational background to the information and data presented in Tables 1−6 and Figures 2−8 is summarized in section 3.1, whereas the description and analysis of these results are included in sections 3.2 and 3.3.

3.1. Computational Approach. A satisfactory description of the entire range of metal−metal interactions in face-shared $[M_2X_9]^{z-}$ dimers can be achieved by means of an approach based on analyzing the broken-symmetry potential energy curves in terms of the curves for the corresponding associated states.[2,4−6]

The molecular structure of face-shared $[M_2Cl_9]^{3-}$ dimers (Figure 1) exhibits an ideal D_{3h} geometry. Imposing symmetry breaking on this structure results in the lowering of the molecular symmetry from D_{3h} to C_{3v} as a consequence of removing all symmetry elements connecting the metal centers. The correlation between C_{3v} and D_{3h} molecular orbital descriptions is shown in Figure 2.

The connection between the (C_{3v}) broken-symmetry and the (D_{3h}) associated states can be made by noting that when antiferromagnetic coupling within a subset of electrons is weak, then the corresponding ferromagnetic associated state,

Table 1. Electronic Configurations and Multiplets Arising from the Different Coupling Modes of d^4d^4 $[M_2Cl_9]^{3-}$ Systems[a]

coupling mode[b]		spin state	configuration	multiplets
$[e^2 \times e^2]$		$S = 0$	$[(a_1')^2(e')^4(e'')^0(a_2'')^2]$	$\mathbf{^1A_1'}$
		$S = 2$	$[(a_1')^2(e')^2(e'')^2(a_2'')^2]$	$\mathbf{^5A_1'}$
$[a_1e \times a_1e]$	low spin	$S = 0$	$[(a_1')^2(e')^4(e'')^2(a_2'')^0]$	$^1E' + {}^1A_1'$
		$S = 1$	$[(a_1')^2(e')^3(e'')^3(a_2'')^0]$	$^3A_1'' + {}^3A_2'' + {}^3E''$
		$S = 2$	$[(a_1')^1(e')^3(e'')^3(a_2'')^1]$	$^5A_1' + {}^5A_2' + {}^5E'$
		$S = 1'$	$[(a_1')^2(e')^4(e'')^2(a_2'')^0]$	$\mathbf{^3A_2'}$
	high spin	$S = 4$	$[(a_1')^1(e')^2(e'')^2(a_2'')^1\text{-}(e')^2(e'')^0]$	$\mathbf{^9A_1'}$
$[a_1e \times e^2]$		$S = 0'$	$[(a_1')^2(e')^4(e'')^1(a_2'')^1]$	$^1E'$
		$S = 1'$	$[(a_1')^2(e')^4(e'')^1(a_2'')^1]$	$\mathbf{^3E'}$
		$S = 2'$	$[(a_1')^2(e')^3(e'')^2(a_2'')^1]$	$\mathbf{^5E'}$

[a] The energy of the multiplets highlighted in bold can be calculated using a single-determinant approach. [b] The notation used corresponds to the "hole configuration" of the metal centers.

where the weakly coupled electrons are aligned in parallel, must lie close in energy. The most representative example is probably found for the d^3d^3 $[M_2X_9]^{z-}$ dimers.[2−4] In these systems, the associated states arise from successive decoupling of the σ and δ_π subsets of electrons and correspond to $S = 0$, $S = 2$, and $S = 3$ configurations, all of which can be represented by single-determinant wave functions. The $S = 0$, $S = 2$, and $S = 3$ states are characterized, respectively, by delocalization of all electrons, delocalization of the σ, but not δ_π, electrons, and localization of all electrons.

The broken-symmetry and spin states which are most relevant to the discussion and analysis of the electronic structures of the Mn, Tc, and Re d^4d^4 face-shared $[M_2Cl_9]^{3-}$ systems are described in Table 1 and Figures 3 and 4.

In cases where the individual metal centers adopt low-spin configurations, a number of coupling modes and spin states arise as a consequence of the fact that the t_{2g} set of orbitals in an ideal octahedral ($[MCl_6]^{3-}$) arrangement is split into a_1 and e subsets by the local C_{3v} symmetry of the metal sites in the $[M_2Cl_9]^{3-}$ dimer, and different occupation patterns are possible. The analysis of these coupling modes and spin states in the d^4d^4 systems becomes analogous to that carried out for d^2d^2 systems in a previous publication,[5] if holes are considered instead of electrons. (The notation for the coupling modes used throughout the text is based on the "hole configuration" of the individual metal centers.)

Three coupling modes can be described for d^4d^4 $[M_2Cl_9]^{3-}$ species by considering that the electron holes associated with the individual metal centers can reside in both the a_1 and e orbitals, or exclusively in the e orbitals. Two symmetric coupling modes (denoted $[e^2 \times e^2]$ and $[a_1e \times a_1e]$), and one asymmetric coupling mode (denoted $[a_1e \times e^2]$), are possible. The corresponding electronic configurations are schematically represented in Figure 3.

In the $[e^2 \times e^2]$ coupling mode, the individual metal centers have an $[(a_1)^2(e)^2]$ configuration, corresponding to two holes in the e orbitals, and the broken-symmetry state is defined by the $[(a_1\uparrow)^1(a_1\downarrow)^1(e\uparrow)^2(e\downarrow)^2(e\uparrow)^0(e\downarrow)^0(a_1\uparrow)^1(a_1\downarrow)^1]$ configuration. Coupling between the δ_π electrons results in $S = 0$, $S = 1$, and $S = 2$ states of $^1A_1'$, $^3A_2''$, and $^5A_1'$ symmetry, respectively. The potential energy curve for the broken-symmetry state can be analyzed in terms of the $S = 0$ and $S = 2$ associated states (Table 1 and Figure 3) corresponding to the $^1A_1'$and $^5A_1'$ multiplets, which arise from antiferromagnetic and ferromagnetic alignment of the δ_π electrons, respectively. This is the simplest coupling mode for the d^4d^4 $[M_2Cl_9]^{3-}$ systems as the $S = 0$ and $S = 2$ states can be described by single-determinant wave functions.

In the $[a_1e \times a_1e]$ coupling mode, the configuration of the individual metal centers is $[(a_1)^1(e)^3]$, corresponding to one hole in each of the a_1 and e orbitals. The resulting broken-symmetry state is represented by the $[(a_1\uparrow)^1(a_1\downarrow)^1(e\uparrow)^2(e\downarrow)^2(e\uparrow)^1(e\downarrow)^1(a_1\uparrow)^0(a_1\downarrow)^0]$ configuration, and three associated states, denoted $S = 0$, $S = 1$, and $S = 2$ (Table 1 and Figure 3), can be defined. The $S = 0$ and $S = 2$ states arise, respectively, from antiferromagnetic and ferromagnetic alignment of the unpaired σ and δ_π electrons, whereas the $S = 1$ state derives from ferromagnetic coupling of the unpaired δ_π electrons exclusively.

Unlike the $[e^2 \times e^2]$ coupling mode, each of the configurations shown in Figure 3 for the $S = 0$, $S = 1$, and $S = 2$ associated states belonging to the $[a_1e \times a_1e]$ coupling mode span more than one multiplet of the same spin. Consequently, the associated states cannot be described by single-determinant wave functions. However, within density functional theory, it is (in principle) possible to calculate the energy of these states by means of the sum method.[15] This approach relies on the principle that the energy of a single determinant can be expressed as a weighted sum of energies of all multiplets arising from the same configuration. In practice, this is only possible if the number of determinants of different energy is the same as the number of multiplets of different energy.

The sum method cannot be used to determine the energies of the $S = 1$ and $S = 2$ associated states because in both cases the number of determinants of different energy is smaller than the number of multiplets, but it can be applied to the $S = 0$ associated state corresponding to the $[(a_1')^2(e')^4(e'')^2]$ singlet configuration shown in Figure 3.[5] This configuration does not correspond to a pure spin state as it contributes to $^3A_2'(M_s = 0) + {}^1E' + {}^1A_1'$ multiplets, but the multiplet energies can be expressed in terms of the energies of the following linear combinations of single determinants:

$$E(^3A_2') = E|(a_1'^{+})(a_1'^{-})(e'^{+})^2(e'^{-})^2(e''_a{}^{+})(e''_b{}^{+})| \quad (1)$$

$$E(^1E') = 2E|(a_1'^{+})(a_1'^{-})(e'^{+})^2(e'^{-})^2(e''_a{}^{+})(e''_b{}^{-})| - E|(a_1'^{+})(a_1'^{-})(e'^{+})^2(e'^{-})^2(e''_a{}^{+})(e''_b{}^{+})| \quad (2)$$

$$E(^1A_1') = 2E|(a_1'^{+})(a_1'^{-})(e'^{+})^2(e'^{-})^2(e''_a{}^{+})(e''_a{}^{-})| - 2E|(a_1'^{+})(a_1'^{-})(e'^{+})^2(e'^{-})^2(e''_a{}^{+})(e''_b{}^{-})| + E|(a_1'^{+})(a_1'^{-})(e'^{+})^2(e'^{-})^2(e''_a{}^{+})(e''_b{}^{+})| \quad (3)$$

The energy of each single determinant is calculated using C_{2v} symmetry (instead of the full D_{3h} symmetry) in order to distinguish between the two components of the e″ orbitals, denoted e''_a and e''_b in eqs 1−3.

(15) Ziegler, T.; Rauk, A.; Baerends, E. J. *Theor. Chim. Acta* **1977**, *43*, 261.

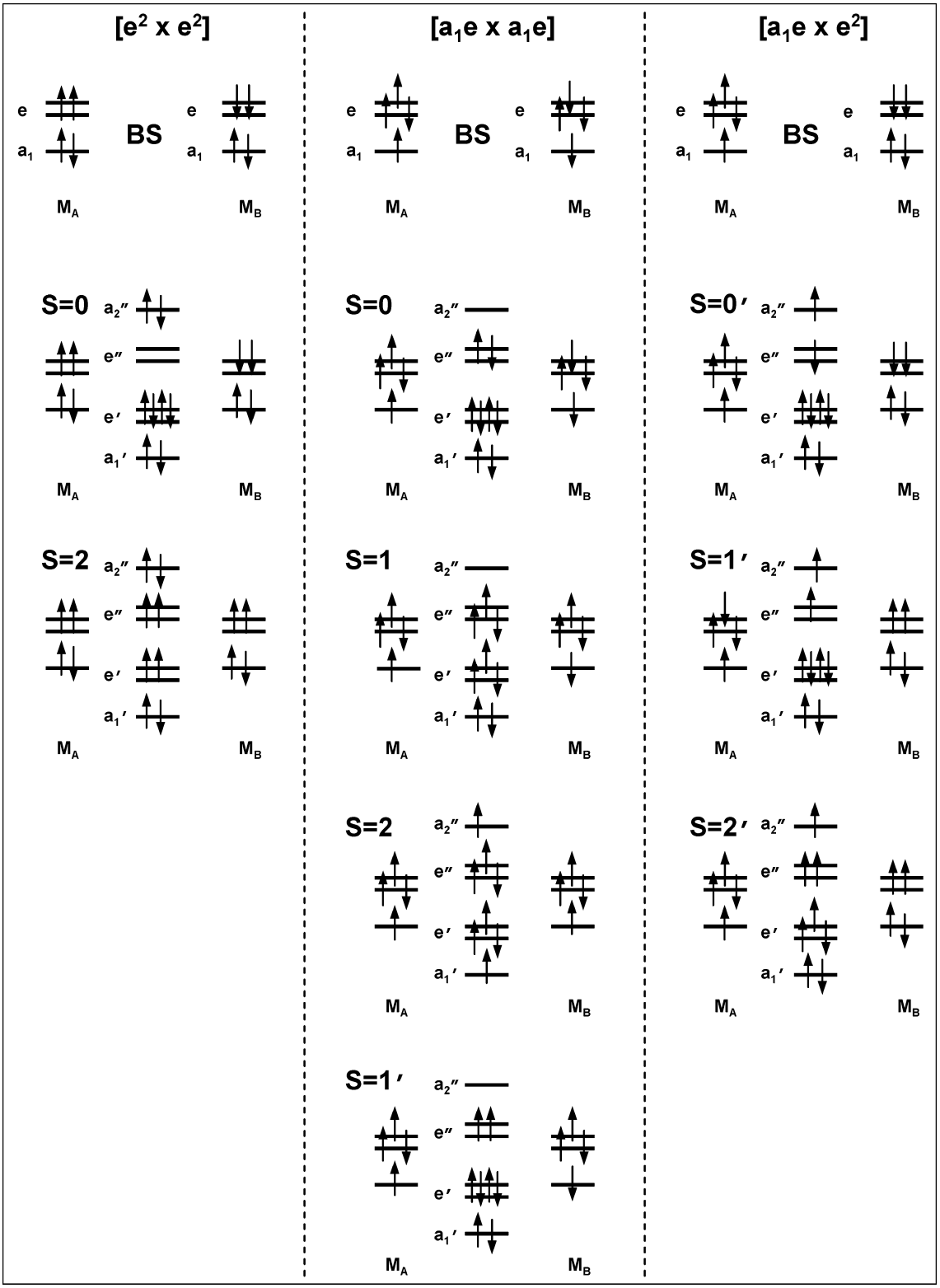

Figure 3. Schematic representation of the electronic configurations for the broken symmetry and spin states in the $[e^2 \times e^2]$, $[a_1e \times a_1e]$, and $[a_1e \times e^2]$ coupling modes of d^4d^4 $[M_2Cl_9]^{3-}$ systems.

An additional (delocalized) triplet state, denoted $S = 1'$ in Table 1 and Figure 3, can be defined in the $[a_1e \times a_1e]$ coupling mode. This state corresponds to the unpaired δ_π electrons occupying the e″ level, as distinct from the $S = 1$ associated state where the unpaired δ_π electrons occupy both the e′ and e″ orbitals. Unlike the $S = 0$, $S = 1$, and $S = 2$ associated states, the $S = 1'$ state can be represented by a single-determinant wave function.

In the asymmetric $[a_1e \times e^2]$ coupling mode, the individual metal centers possess different configurations corresponding, respectively, to $[(a_1)^1(e)^3]$ (with one hole in each of the a_1 and e orbitals) and $[(a_1)^2(e)^2]$ (with two holes in the e

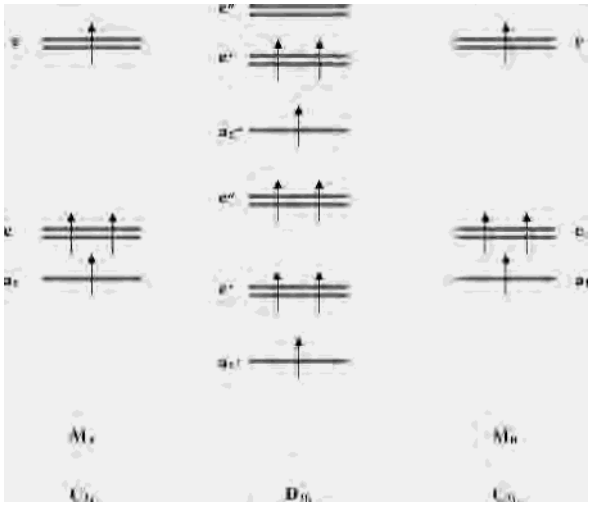

Figure 4. Schematic representation of the electronic configurations for the $S = 4$ state of d^4d^4 $[M_2Cl_9]^{3-}$ systems.

orbitals). The broken-symmetry state for this coupling mode is defined by the $[(a_1\uparrow)^1(a_1\downarrow)^1(e\uparrow)^2(e\downarrow)^2(e\uparrow)^0(e\downarrow)^1(a_1\uparrow)^1(a_1\downarrow)^0]$ configuration, but no associated states can be considered as the coupling involves different subsets of electrons on opposite metal centers. However, three delocalized states, denoted $S = 0'$, $S = 1'$, and $S = 2'$ in Table 1 and Figure 3, can be defined.

Analogously to the $[a_1e \times a_1e]$ coupling mode, the $S = 0'$ spin state cannot be described in terms of a single-determinant wave function, but the sum method can be used to determine the energy of the $^1E' + {}^3E'(M_s = 0)$ multiplets corresponding to this singlet configuration.[5] The energies of these multiplets can be expressed in terms of the following combinations of single determinants:

$$E(^3E') = E|(a_1'^+)(a_1'^-)(e'^+)^2(e'^-)^2(e''_a{}^+)(a_2''^+)| \quad (4)$$

$$E(^1E') = 2E|(a_1'^+)(a_1'^-)(e'^+)^2(e'^-)^2(e''_a{}^-)(a_2''^+)| - E|(a_1'^+)(a_1'^-)(e'^+)^2(e'^-)^2(e''_a{}^+)(a_2''^+)| \quad (5)$$

The energy of each single determinant is also calculated using C_{2v} symmetry in order to distinguish between the two components of the e″ orbitals.

An $S = 4$ state is also possible for d^4d^4 $[M_2Cl_9]^{3-}$ systems (Table 1 and Figure 4). This state corresponds to the individual metal centers adopting high-spin $[(a_1)^1(e)^2(e)^1]$ configurations (in C_{3v} symmetry).

The $S = 4$ state can be connected with a broken-symmetry configuration equivalent to that for the $[a_1e \times a_1e]$ coupling mode. This is a consequence of the fact that both e′ and e″ (D_{3h}) orbitals transform as the e (C_{3v}) irreducible representation when the molecular symmetry is reduced from D_{3h} to C_{3v}. Thus, the broken-symmetry configurations for the (low-spin) $[a_1e \times a_1e]$ states and for the $S = 4$ state are both characterized by an overall electron distribution corresponding to an $[(a_1)^2(e)^4(e)^2]$ occupancy. This broken-symmetry configuration can, therefore, encompass the description of both low-spin and high-spin cases.

3.2. Potential Energy Curves. Optimized metal−metal distances and total bonding energies corresponding to the minima in the potential energy curves, for all the broken-symmetry and spin states of the Mn, Tc, and Re systems (which have been investigated in the present work), are summarized in Tables 2−4.

Table 2. Optimized Metal−Metal Bond Distance (M−M in Å) and Total Bonding Energy (E_B in eV) for the Various States of $[Re_2Cl_9]^{3-}$

coupling mode		state	M−M	E_B
$[e^2 \times e^2]$		BS	3.401	−50.67
		$S = 0$	2.843	−49.35
		$S = 2$	3.362	−50.59
$[a_1e \times a_1e]$	low spin	BS	2.588	−51.52
		$S = 0$ (E′)	2.560	−51.49
		$S = 0$ (A_1')	2.563	−51.41
		$S = 1$	2.838	−51.37
		$S = 2$	3.353	−50.62
		$S = 1'$	2.571	−51.78
	high spin	$S = 4$	3.805	−48.73
$[a_1e \times e^2]$		BS	3.218	−50.93
		$S = 0'$	2.683	−50.46
		$S = 1'$	2.700	−50.76
		$S = 2'$	2.962	−51.16

Table 3. Optimized Metal−Metal Bond Distance (M−M in Å) and Total Bonding Energy (E_B in eV) for the Various States of $[Tc_2Cl_9]^{3-}$

coupling mode		state	M−M	E_B
$[e^2 \times e^2]$		BS	3.337	−50.59
		$S = 0$	2.849	−49.12
		$S = 2$	3.301	−50.53
$[a_1e \times a_1e]$	low spin	BS	2.670	−51.11
		$S = 0$ (E′)	2.537	−51.08
		$S = 0$ (A_1')	2.514	−50.94
		$S = 1$	2.740	−51.07
		$S = 2$	3.293	−50.56
		$S = 1'$	2.570	−51.41
	high spin	$S = 4$	3.724	−49.13
$[a_1e \times e^2]$		BS	3.152	−50.79
		$S = 0'$	2.645	−50.13
		$S = 1'$	2.653	−50.47
		$S = 2'$	2.936	−51.04

Table 4. Optimized Metal−Metal Bond Distance (M−M in Å) and Total Bonding Energy (E_B in eV) for the Various States of $[Mn_2Cl_9]^{3-}$

coupling mode		state	M−M	E_B
$[e^2 \times e^2]$		BS	3.105	−47.82
		$S = 0$	3.021	−45.67
		$S = 2$	3.101	−47.82
$[a_1e \times a_1e]$	low spin	BS	3.303	−48.91
		$S = 0$ (E′)	2.501	−46.69
		$S = 0$ (A_1')	2.517	−46.13
		$S = 1$	2.688	−47.21
		$S = 2$	3.101	−47.84
		$S = 1'$	2.500	−47.26
	high spin	$S = 4$	3.433	−48.93
$[a_1e \times e^2]$		BS	3.047	−47.94
		$S = 0'$	2.716	−46.16
		$S = 1'$	2.722	−46.77
		$S = 2'$	2.878	−48.08

The potential energy curves for the various states connected with the three coupling modes described in Section 3.1 are shown in Figure 5 for the Re system, whereas the potential energy curves for the states which are most important for the determination of the global minima of $[Mn_2Cl_9]^{3-}$, $[Tc_2Cl_9]^{3-}$, and $[Re_2Cl_9]^{3-}$, and for a comparative discussion of the similarities and differences observed, are collected in Figure 6.

3.2.1. Coupling Modes and Potential Energy Curves for $[Re_2Cl_9]^{3-}$. Potential energy curves for the states cor-

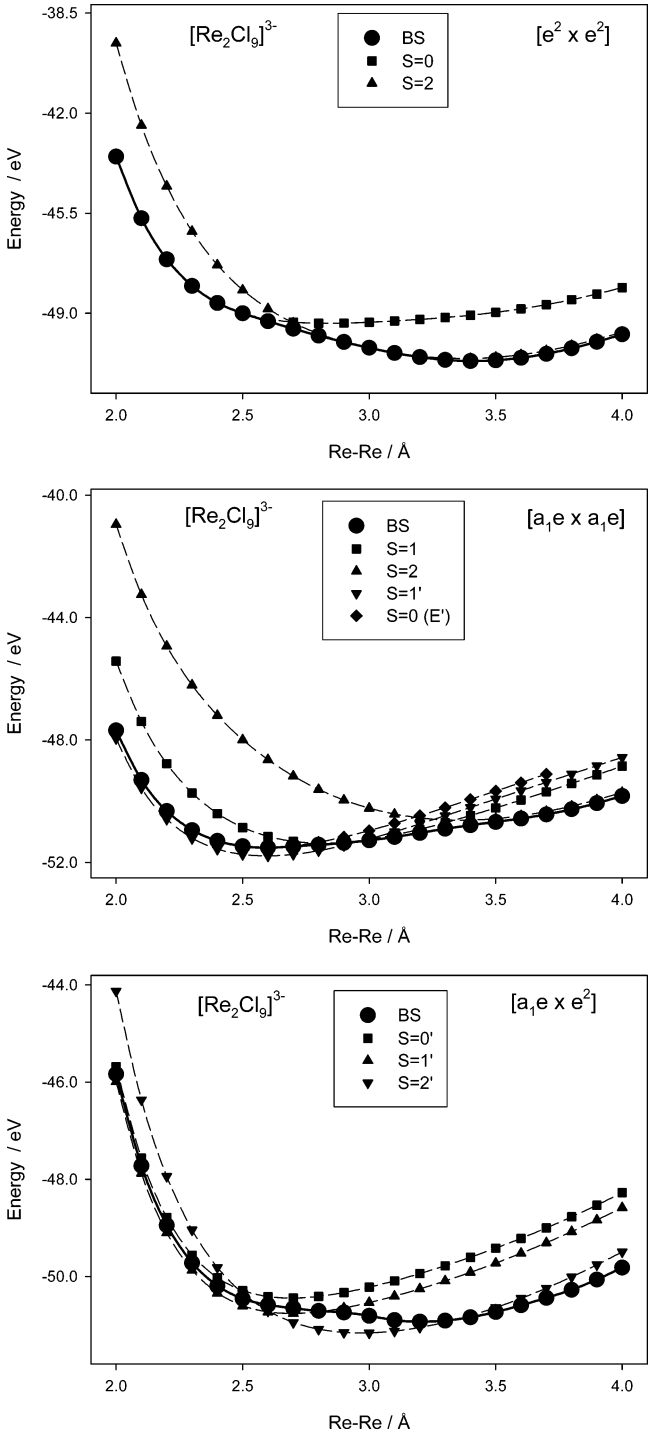

Figure 5. Potential energy curves for $[Re_2Cl_9]^{3-}$.

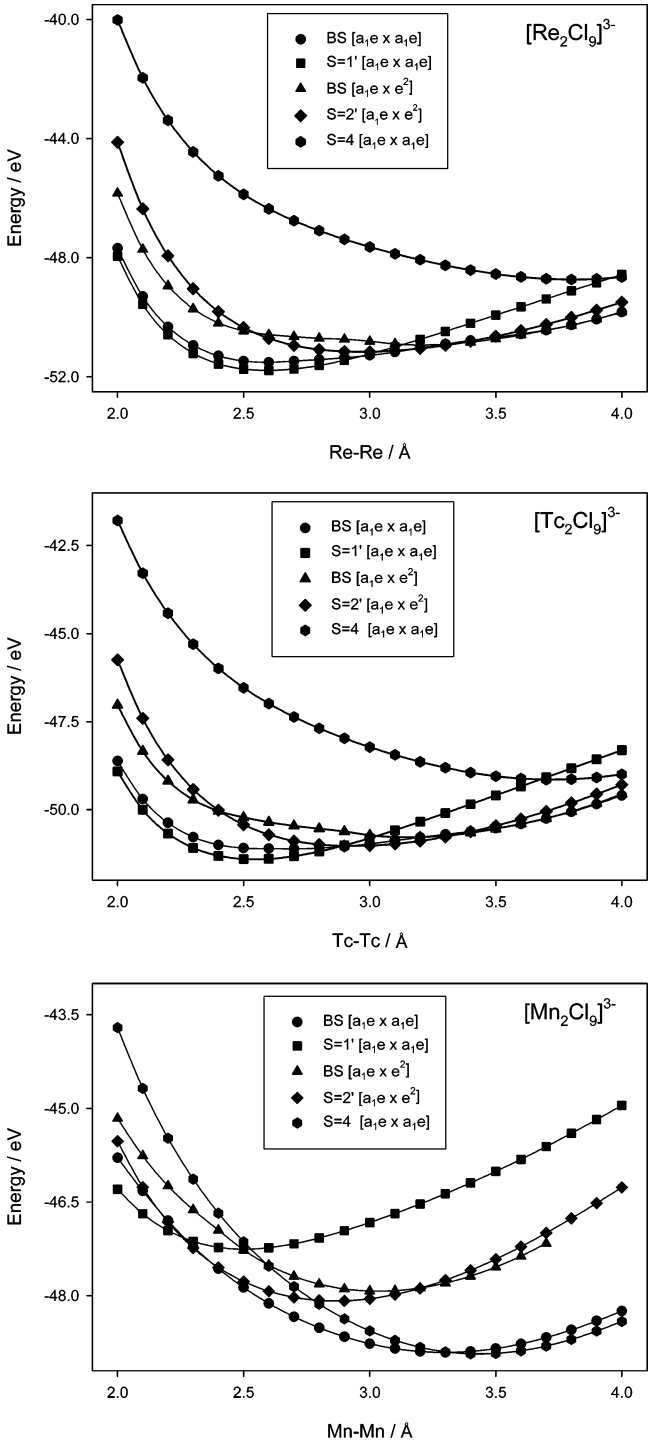

Figure 6. Potential energy curves for $[Mn_2Cl_9]^{3-}$, $[Tc_2Cl_9]^{3-}$, and $[Re_2Cl_9]^{3-}$.

responding to the $[e^2 \times e^2]$, $[a_1e \times a_1e]$, and $[a_1e \times e^2]$ coupling modes of the individual metal centers, in the Re system, are shown in Figure 5.

In the $[e^2 \times e^2]$ coupling mode, the broken-symmetry state lies close to the $S = 2$ state at intermediate to long metal−metal distances but converges to the $S = 0$ state at shorter metal−metal separations. At the respective optimized bond lengths, the $S = 2$ state is significantly lower in energy than the $S = 0$ state, and the global minimum in the broken-symmetry curve, which occurs at 3.40 Å, is almost coincident with that of the $S = 2$ curve, indicating that localization of the metal-based electrons is a predominant feature in the broken-symmetry state for this coupling mode.

In the $[a_1e \times a_1e]$ coupling mode, the broken-symmetry curve lies close to the $S = 2$ state at long metal−metal distances, indicating electron localization, whereas at short metal−metal distances, it converges to the $S = 0$ state where complete electron delocalization occurs as a result of the formation of σ (a_1') and δ_π (e′) bonds. In the intermediate range of metal−metal separations, the $S = 1$ state lies lower

in energy than both the $S = 0$ and $S = 2$ states, and closest to the broken-symmetry curve. Therefore, at intermediate Re−Re distances, the metal−metal interactions can be described as involving a σ bond, but only weakly coupled δ_π electrons. At Re−Re distances of approximately 2.55−2.65 Å, the minimum in the broken-symmetry curve for the $[a_1e \times a_1e]$ coupling mode coincides with that of the $S = 0$ state corresponding to formation of a metal−metal double bond. However, the global minimum for this coupling mode corresponds to the delocalized $S = 1'$ state (also characterized by a Re−Re double bond) at a metal−metal bond length of 2.57 Å.

In the $[a_1e \times e^2]$ coupling mode, the potential energy curves for the broken-symmetry, $S = 0'$, and $S = 1'$ states lie parallel to one another at short metal−metal distances, with the $S = 1'$ curve exhibiting the lowest energy. At longer metal−metal separations, the $S = 0'$ and $S = 1'$ curves remain parallel to each other, but the broken-symmetry curve shifts to significantly lower energy and, at long Re−Re distances, lies close to the $S = 2'$ state. The potential energy curve for the $S = 2'$ state exhibits the lowest energy in the intermediate range of metal−metal separations, and represents the global minimum for the $[a_1e \times e^2]$ coupling mode at a Re−Re distance of 2.96 Å.

3.2.2. General Analysis of the Potential Energy Curves. The potential energy curves for the various coupling modes and states of $[Re_2Cl_9]^{3-}$ and $[Tc_2Cl_9]^{3-}$ are qualitatively similar, as the behavior of both systems is characterized by a strong preference for the states where the metal centers adopt low-spin configurations. As found for the Re system, the global minima for the $[e^2 \times e^2]$, $[a_1e \times a_1e]$, and $[a_1e \times e^2]$ coupling modes of $[Tc_2Cl_9]^{3-}$ correspond, respectively, to $S = 2$, $S = 1'$, and $S = 2'$ states (but occur at slightly shorter metal−metal separations than for $[Re_2Cl_9]^{3-}$).

The potential energy curves for the states which are most important in determining the global minimum for the Re and Tc systems are collected in Figure 6. The $S = 4$ state, where the metal centers adopt high-spin configurations, is also included for comparison.

For both $[Re_2Cl_9]^{3-}$ and $[Tc_2Cl_9]^{3-}$, the global minimum occurs at a metal−metal separation of 2.57 Å and corresponds to the $S = 1'$ state belonging to the $[a_1e \times a_1e]$ coupling mode. The metal−metal interaction at this minimum is best described as complete electron delocalization in a Re−Re or Tc−Tc double (σ and δ_π) bond. The potential energy curve for this state is the lowest-lying curve at metal−metal distances shorter than approximately 2.8−2.9 Å, but it shifts to higher energy as the metal−metal separation increases. In $[Re_2Cl_9]^{3-}$, the broken-symmetry states arising from the $[a_1e \times a_1e]$ and $[a_1e \times e^2]$ coupling modes become the lowest-lying curves at Re−Re distances longer than 3.0 Å. In $[Tc_2Cl_9]^{3-}$, the $S = 2'$ state arising from the $[a_1e \times e^2]$ coupling mode becomes the lowest-lying curve at Tc−Tc distances between approximately 2.9 and 3.3 Å. Beyond 3.4 Å, the broken-symmetry curves associated with the $[a_1e \times a_1e]$ and $[a_1e \times e^2]$ coupling modes lie lowest in energy, analogously to $[Re_2Cl_9]^{3-}$. The $S = 4$ state lies at relatively high energy throughout the entire range of metal−metal distances investigated and is not an option for the ground state of the Re and Tc systems.

In general, the potential energy curves for $[Mn_2Cl_9]^{3-}$ exhibit significant differences from those obtained for $[Tc_2Cl_9]^{3-}$ and $[Re_2Cl_9]^{3-}$, and unlike the heavier members of the group, the states associated with the individual metal centers adopting high-spin configurations play a central role in determining the global minimum for the Mn system.

The potential energy curves for the states which are most relevant to determining the global minimum of $[Mn_2Cl_9]^{3-}$ are also shown in Figure 6. Unlike the Tc and Re systems, where the lowest energy state corresponds to electron delocalization in a relatively short metal−metal double bond, the global minimum in $[Mn_2Cl_9]^{3-}$ occurs at the rather long Mn−Mn separation of 3.43 Å, corresponding to the $S = 4$ state. This global minimum can be characterized as involving a localized electron distribution with the weakly coupled metal centers adopting high-spin configurations.

The $S = 4$ state represents the lowest-lying potential energy curve at Mn−Mn distances longer than 3.3 Å, whereas the broken-symmetry state for the $[a_1e \times a_1e]$ coupling mode and the $S = 2'$ state arising from the $[a_1e \times e^2]$ coupling mode lie lowest in energy at shorter metal−metal separations. The delocalized $S = 1'$ state belonging to the $[a_1e \times a_1e]$ coupling mode represents the global minimum for the Re and Tc systems, but for $[Mn_2Cl_9]^{3-}$, it becomes the lowest-lying curve only at the shortest metal−metal separations investigated.

In principle, monomeric six-coordinate Mn species possessing a high-spin d^4 configuration are subject to the Jahn−Teller effect due to the orbital degeneracy arising from the $[t_{2g}^3e_g^1]$ d-orbital occupancy. In $[MnCl_6]^{3-}$, for example, a distorted D_{4h} structure is significantly more stable than the regular O_h geometry. Although the individual Mn centers in $[Mn_2Cl_9]^{3-}$ possess local C_{3v} symmetry, a Jahn−Teller distortion is possible due to the orbital degeneracy arising from the $[(a_1)^1(e)^2(e)^1]$ configuration of the individual metal centers in the $S = 4$ state of the dimer. This possibility has been explored by lowering the molecular symmetry to C_s (and thus removing the orbital degeneracy), but the calculations have revealed only minor geometrical changes, with the local C_{3v} and overall D_{3h} (dimer) symmetries largely retained.

3.3. Energy Parameters and Electronic Structure of $[MCl_6]^{3-}$ and $[M_2Cl_9]^{3-}$ Systems. In our study[7] of the d^5d^5 $[M_2Cl_9]^{3-}$ species of Fe, Ru, and Os, closed energy cycles were used in order to obtain a quantitative measure of the preference for localized or delocalized electron distributions and high-spin or low-spin configurations in these systems. This approach is applied in the present investigation to the d^4d^4 $[M_2Cl_9]^{3-}$ species of Mn, Tc, and Re.

For comparison, a closed energy cycle for the octahedral $[MCl_6]^{3-}$ monomers is defined in section a of Figure 7. The equilibrium energy between the high-spin and low-spin

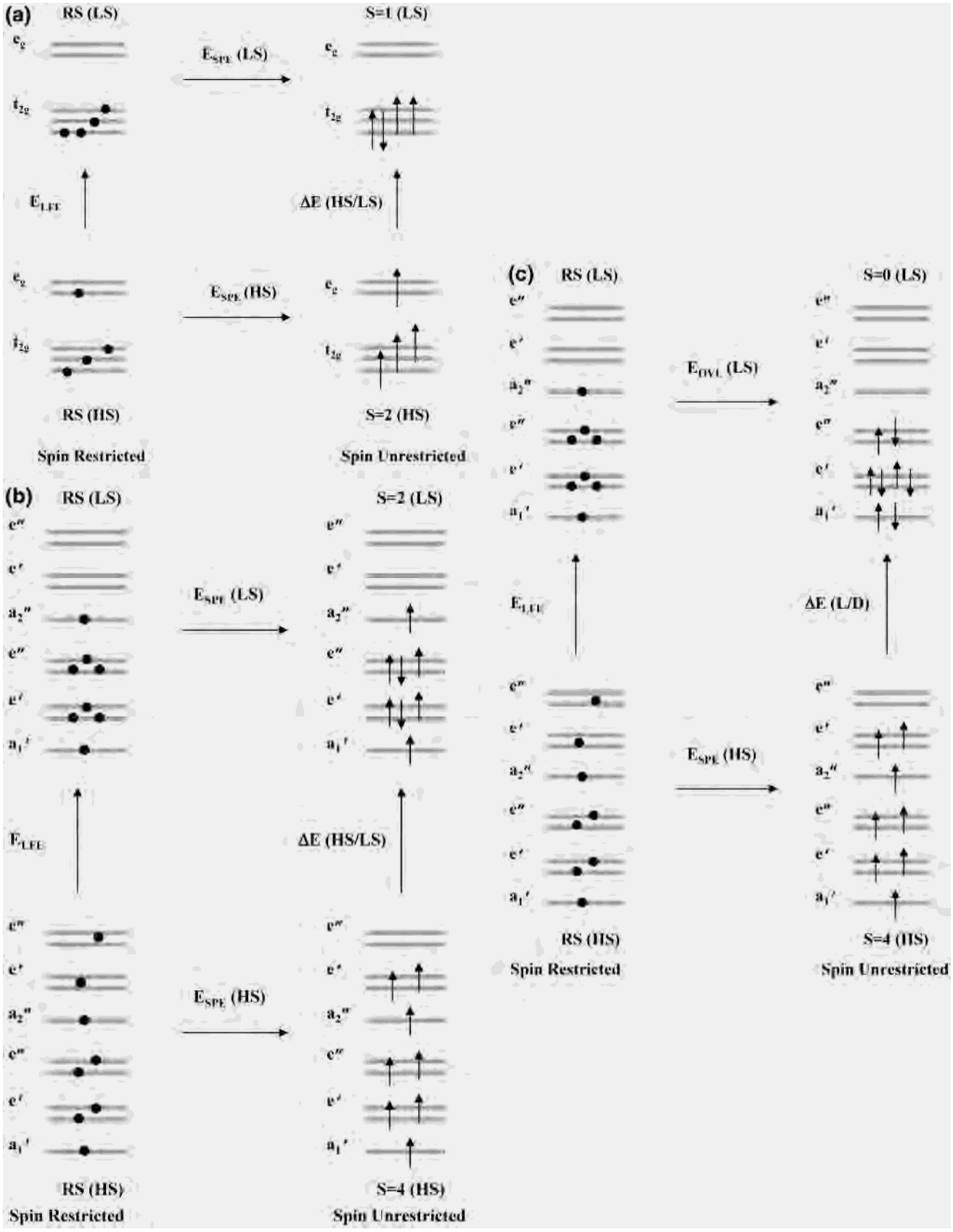

Figure 7. Energy cycles for (a) high-spin/low-spin equilibrium in octahedral d^4 $[MCl_6]^{3-}$ species, (b) high-spin/low-spin equilibrium in d^4d^4 $[M_2Cl_9]^{3-}$ species, (c) localization/delocalization equilibrium in d^4d^4 $[M_2Cl_9]^{3-}$ species.

configurations (denoted ΔE(HS/LS)), the ligand-field energy (denoted E_{LFE}), and the spin polarization energy for high-spin and low-spin configurations (denoted E_{SPE}(HS) and E_{SPE}(LS), respectively) can be derived from the four states

Table 5. Energy Parameters (in eV) for d^4 $[MCl_6]^{3-}$ Species

energy term	$[MnCl_6]^{3-}$	$[TcCl_6]^{3-}$	$[ReCl_6]^{3-}$
$E_{SPE}(LS)$	+0.83	+0.48	+0.42
$E_{SPE}(HS)$	+2.82	+1.63	+1.42
E_{LFE}	+1.26	+1.77	+1.89
$\Delta E(HS/LS)$	−0.73	+0.62	+0.89

contained in the cycle, as follows:

$$E_{LFE} = E_{RS}(HS) - E_{RS}(LS) \quad (6)$$

$$E_{SPE}(LS) = E_{RS}(LS) - E(S = 1) \quad (7)$$

$$E_{SPE}(HS) = E_{RS}(HS) - E(S = 2) \quad (8)$$

$$\Delta E(HS/LS) = E(S = 2) - E(S = 1) = E_{LFE} + E_{SPE}(LS) - E_{SPE}(HS) \quad (9)$$

The ligand field term takes account of the energy required to promote an electron from the t_{2g} to e_g orbitals and also includes the difference in Coulombic repulsion between the high-spin and low-spin configuration, whereas the spin polarization terms reflect the energetic difference between the spin-restricted and spin-unrestricted calculations for each configuration.

The reference states (denoted RS) correspond to the $[t_{2g}^3e_g^1]$ (high-spin) and $[t_{2g}^4e_g^0]$ (low-spin) configurations, and their energies are calculated in a spin-restricted manner. (The circles in the energy-level diagrams of Figure 7 are intended to indicate that electron spin is undefined.) The states that define the high-spin/low-spin equilibrium are characterized by the $[(t_{2g}\uparrow)^3(t_{2g}\downarrow)^1(e_g\uparrow)^0(e_g\downarrow)^0]$ low-spin ($S = 1$) and $[(t_{2g}\uparrow)^3(t_{2g}\downarrow)^0(e_g\uparrow)^1(e_g\downarrow)^0]$ high-spin ($S = 2$) configurations, respectively.

The calculated values of the ligand-field, spin polarization, and high-spin/low-spin equilibrium terms for the $[MCl_6]^{3-}$ species are summarized in Table 5. A considerable increase in the ligand-field energy is observed between the Mn and Tc complexes, but the results are much more similar for the Tc and Re species. This trend can be rationalized in terms of the greater radial extension of the 4d and 5d orbitals in Tc and Re relative to the 3d orbitals in Mn. The spin polarization terms display an opposite (but qualitatively similar) trend, a significant reduction in the energy values being observed from $[MnCl_6]^{3-}$ to $[TcCl_6]^{3-}$, but a rather smaller difference found between $[TcCl_6]^{3-}$ and $[ReCl_6]^{3-}$.

In $[MnCl_6]^{3-}$, a high-spin configuration is favored, as indicated by the negative value of the ΔE(HS/LS) term, as a consequence of the large high-spin polarization energy exhibited by this species. In $[TcCl_6]^{3-}$ and $[ReCl_6]^{3-}$, the combined effect of the larger ligand-field terms and lower values for the high-spin polarization energy results in a preference for low-spin configurations in these systems, as reflected by the positive values of the ΔE(HS/LS) term.

Closed energy cycles for the high-spin/low-spin and localization/delocalization equilibria in $[M_2Cl_9]^{3-}$ species are defined in sections b and c of Figure 7, respectively. In our previous studies[3,16] of $[M_2X_9]^{z-}$ systems, we have identified two factors as central to determining the strength of the metal−metal interactions. These are the overlap between the orbitals on opposite metal centers, and the spin polarization energy associated with the presence of unpaired electron density on the metal sites. Significant overlap of the metal orbitals favors electron delocalization, whereas the spin polarization energy favors electron localization.

In systems where the individual metal centers possess low-spin configurations, the orbital overlap and spin polarization terms can be obtained, respectively, from the energetic difference between the $S = 0$ and $S = 2$ states and a low-spin reference state defined so that the contributions from orbital overlap and spin polarization are canceled. The energy of this reference state can be determined by performing a spin-restricted calculation on an electronic configuration in which bonding and antibonding orbitals are evenly occupied. For the d^4d^4 $[M_2Cl_9]^{3-}$ species, this configuration is represented by $[(a_1'\uparrow)^{1/2}(a_1'\downarrow)^{1/2}(e'\uparrow)^{3/2}(e'\downarrow)^{3/2}(e''\uparrow)^{3/2}(e''\downarrow)^{3/2}(a_2''\uparrow)^{1/2}(a_2''\downarrow)^{1/2}]$.

The orbital overlap (E_{OVL}) and spin polarization energy terms for low-spin configurations can therefore be written as

$$E_{OVL}(LS) = E_{RS}(LS) - E(S = 0) \quad (10)$$

$$E_{SPE}(LS) = E_{RS}(LS) - E(S = 2) \quad (11)$$

The $S = 0$ state corresponds to the $[(a_1'\uparrow)^1(a_1'\downarrow)^1(e'\uparrow)^2(e'\downarrow)^2(e''\uparrow)^1(e''\downarrow)^1(a_2''\uparrow)^0(a_2''\downarrow)^0]$ configuration, whereas the $S = 2$ state is characterized by the $[(a_1'\uparrow)^1(a_1'\downarrow)^0(e'\uparrow)^2(e'\downarrow)^1(e''\uparrow)^2(e''\downarrow)^1(a_2''\uparrow)^1(a_2''\downarrow)^0]$ configuration.

The high-spin reference state and the $S = 4$ state are defined, respectively, by the $[(a_1'\uparrow)^{1/2}(a_1'\downarrow)^{1/2}(e'\uparrow)^1(e'\downarrow)^1(e''\uparrow)^1(e''\downarrow)^1a_2''\uparrow)^{1/2}(a_2''\downarrow)^{1/2}(e'\uparrow)^{1/2}(e'\downarrow)^{1/2}(e''\uparrow)^{1/2}e''\downarrow)^{1/2}]$ and $[(a_1'\uparrow)^1(a_1'\downarrow)^0(e'\uparrow)^2(e'\downarrow)^0(e''\uparrow)^2(e''\downarrow)^0\ (a_2''\uparrow)^1(a_2''\downarrow)^0(e'\uparrow)^2(e'\downarrow)^0(e''\uparrow)^0(e''\downarrow)^0]$ configurations, and the corresponding spin polarization term can be calculated as

$$E_{SPE}(HS) = E_{RS}(HS) - E(S = 4) \quad (12)$$

The definition of the ligand-field energy is analogous to that for the monomeric complexes and corresponds to the difference between the spin-restricted energies of the low-spin and high-spin reference states of the dimer. In the absence of any interaction between the $[MCl_6]^{3-}$ fragments, this term should be approximately twice as large as the monomeric ligand field term.

The high-spin/low-spin, ΔE(HS/LS), and localization/delocalization, ΔE(L/D), equilibrium terms are given by

$$\Delta E(HS/LS) = E(S = 4) - E(S = 2) = E_{LFE} + E_{SPE}(LS) - E_{SPE}(HS) \quad (13)$$

$$\Delta E(L/D) = E(S = 4) - E(S = 0) = E_{LFE} + E_{OVL}(LS) - E_{SPE}(HS) \quad (14)$$

The calculated values of the various energy parameters for $[M_2Cl_9]^{3-}$ species are given in Table 6. The trends in the orbital overlap and spin polarization terms are analogous

(16) Cavigliasso, G.; Stranger, R. *Inorg. Chem.* **2003**, *42*, 5252.

Table 6. Energy Parameters (in eV) for d^4d^4 $[M_2Cl_9]^{3-}$ Species

energy term	$[Mn_2Cl_9]^{3-}$	$[Tc_2Cl_9]^{3-}$	$[Re_2Cl_9]^{3-}$
E_{OVL}(LS)	+0.51	+1.48	+1.71
E_{SPE}(LS)	+1.66	+0.95	+0.83
E_{SPE}(LS) − E_{OVL}(LS)	+1.24	−0.45	−0.81
E_{SPE}(HS)	+5.45	+3.29	+2.94
E_{LFE}	+2.70	+3.75	+4.00
ΔE(HS/LS)	−1.09	+1.41	+1.89
ΔE(L/D)	−2.24	+1.94	+2.77

to those displayed by the d^1d^1, d^2d^2, d^3d^3, and d^5d^5 dimers previously investigated.[3,5,7] Upon descending a transition metal group, the greater size of the metal ions and the more diffuse nature of the metal orbitals lead to an increase in the orbital overlap energy and a reduction in the spin polarization energy.

For low-spin configurations, the difference between the orbital overlap and spin polarization terms (denoted E_{SPE}(LS) − E_{OVL}(LS)) can be used as a measure of the tendency of the metal-based electrons to localize or delocalize. The results in Table 6 indicate that localized electron distributions are more favorable in $[Mn_2Cl_9]^{3-}$, whereas delocalization of the metal-based electrons is favored in $[Tc_2Cl_9]^{3-}$ and $[Re_2Cl_9]^{3-}$. These results are consistent with the nature of the respective potential energy curves shown in Figure 6, which are characterized by a global minimum corresponding to delocalized electrons and a metal−metal double bond in the Tc and Re dimers, but to localized electrons and no metal−metal bond in the Mn species.

In $[MCl_6]^{3-}$ and $[M_2Cl_9]^{3-}$ systems, the spin polarization terms for both the low-spin and high-spin configurations exhibit decreasing trends as the group is descended, and a comparison of the results for the monomer and dimer species reveals that the energy values are related by a factor of approximately 2. Therefore, as found for the various transition metal $[M_2X_9]^{z-}$ systems previously studied,[3,5,7] the spin polarization energy of the dimer appears to be largely determined by the sum of the contributions from the individual metal centers.

We have previously observed[3,16] a strong interdependence between orbital overlap and spin polarization effects in d^3d^3 dimers, for both transition-metal ($[M_2Cl_9]^{z-}$) and halide ($[Mo_2X_9]^{3-}$ and $[W_2X_9]^{3-}$) series. A similar dependence has been noted for the d^5d^5 $[M_2Cl_9]^{3-}$ dimer systems involving Fe, Ru, and Os.[7] Furthermore, for this series, strong linear correlations between the ligand-field and spin polarization terms, and also between the localization/delocalization and high-spin/low-spin equilibrium energy terms, have been found.

Similar trends are evident for the Mn, Tc, and Re d^4d^4 $[M_2Cl_9]^{3-}$ series, as is apparent from the strong linear correlation between the localization/delocalization and high-spin/low-spin equilibrium energy terms observed in Figure 8. Analogously to the d^5d^5 systems, all d^4d^4 dimers fall into diagonally opposite quadrants suggesting that the onset of metal−metal bonding is intimately linked to the high-spin/low-spin crossover in these systems and that neither delocalized high-spin or localized low-spin structures are likely to occur.

The linear dependence between the orbital overlap, ligand-field, and spin polarization terms has been explained[7] by considering that these parameters are all sensitive to the dilation of the metal orbitals. Therefore, as the group is descended, metal−metal overlap and metal−ligand overlap increase due to orbital expansion, whereas the spin polarization energy decreases due to the greater average interelectronic separation. The involvement of the orbital overlap, ligand-field, and spin polarization terms in the expressions for the localization/delocalization and high-spin/low-spin equilibrium energy terms is a possible reason for the linear correlations observed between these two parameters.

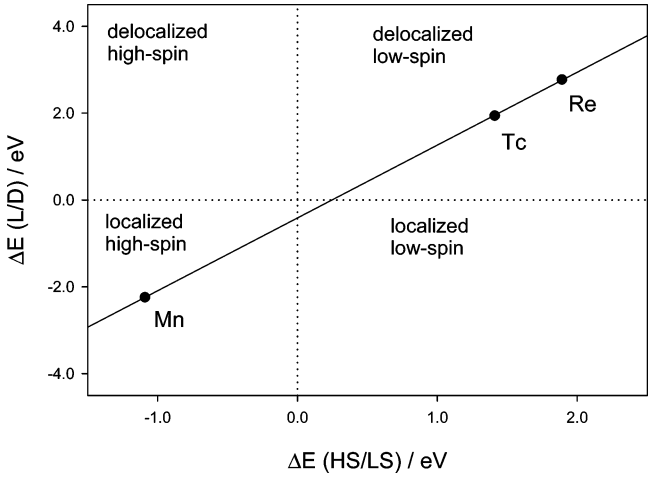

Figure 8. Graphical representation of the variation of the localization/delocalization equilibrium energy as a function of the high-spin/low-spin equilibrium energy, for d^4d^4 $[M_2Cl_9]^{3-}$ species.

4. Conclusion

The electronic structures and metal−metal bonding in Mn, Tc, and Re d^4d^4 $[M_2Cl_9]^{3-}$ systems have been investigated by calculating potential energy curves for various broken-symmetry and spin states arising from the d^4d^4 coupling modes. Closed energy cycles have been utilized to obtain a quantitative measure of the preference for electron localization or delocalization and for high-spin or low-spin configurations in these systems.

The global minima in $[Tc_2Cl_9]^{3-}$ and $[Re_2Cl_9]^{3-}$ correspond to the $S = 1'$ state arising from the $[a_1e \times a_1e]$ coupling mode and involve metal centers with low-spin configurations. This state is characterized by delocalization of the metal-based electrons in relatively short Tc−Tc and Re−Re double (σ and δ_π) bonds. These results can be rationalized on the basis that orbital overlap and ligand-field effects play a more prominent role than spin polarization energy in the Tc and Re dimers, and therefore, the localization/delocalization and high-spin/low-spin equilibria are displaced toward delocalized states and low-spin configurations.

In contrast, the global minimum in $[Mn_2Cl_9]^{3-}$ corresponds to the $S = 4$ state arising from the coupling of metal centers with high-spin configurations and is characterized by localized metal-based electrons and a rather long Mn−Mn separation. This is consistent with the spin polarization energy being quantitatively more important than the orbital overlap and ligand-field terms, resulting in the localization/delocalization and high-spin/low-spin equilibria being dis-

placed in the direction of localized states and high-spin configurations.

We have considered in the Introduction that similarities could be expected between the d^4d^4 systems investigated in the present work and the d^2d^2 and d^5d^5 species previously studied, due to the electron−hole equivalence of the d^2d^2 and d^4d^4 configurations and the fact that both d^4d^4 and d^5d^5 systems involve individual metal centers adopting either high-spin or low-spin configurations.

Similarities between the d^2d^2 and d^4d^4 systems exist in that the global minimum for the d^2d^2 $[Nb_2Cl_9]^{3-}$ and $[Ta_2Cl_9]^{3-}$ dimers, as in the Tc and Re d^4d^4 systems, corresponds to the $S = 1'$ state which arises from the $[a_1e \times a_1e]$ coupling mode and involves delocalized electrons in a metal−metal double (σ and δ_π) bond. In contrast (and analogously to the "low-spin" states of the Mn d^4d^4 dimer), $[V_2Cl_9]^{3-}$ exhibits a global minimum corresponding to the $S = 2'$ state belonging to the $[a_1e \times e^2]$ coupling mode, which is characterized by a relatively long metal−metal separation and weak coupling between the metal-based electrons.

The similarities existing between the d^4d^4 and d^5d^5 systems relate to the observation that the 3d (Mn and Fe) elements show a strong preference for high-spin configurations and electron localization, whereas the 4d (Tc and Ru) and 5d (Re and Os) elements strongly favor low-spin configurations and electron delocalization in metal−metal bonds.

Acknowledgment. Financial support from the Australian Research Council is gratefully acknowledged.

IC0349611